Hidden Heterometallic Interaction Emerges from Resonant Inelastic X-ray Scattering in Luminescent Tb–Pt Molecules

Takefumi Yoshida,[*a,b] *Ahmed Shabana,*[c,d] *David Chukwuma Izuogu,*[e,f] *Kentaro Fuku,*[c] *Tetsu Sato,*[c] *Haitao Zhang,*[c] *Yukina Yamamoto,*[g] *Jun Kamata,*[g] *Hitomi Ohmagari,*[g] *Miki Hasegawa,*[g] *Goulven Cosquer,*[h] *Shinya Takaishi,*[c] *Takuma Kaneko,*[i] *Tomoya Uruga,*[i] *Yasuhiro Iwasawa*[a,b] *and Masahiro Yamashita*[*j, c]

[a] Innovation Research Center for Fuel Cells, The University of Electro-Communications, Chofu, Tokyo 182-8585, Japan. Email: takefumi.yoshida@uec.ac.jp

[b] Physical and Chemical Research Infrastructure Group, RIKEN SPring-8 Center, RIKEN, 1-1-1 Kouto, Sayo-cho, Sayo-gun, Hyogo 679-5148, Japan

[c] Department of Chemistry, Graduate School of Science Tohoku University, 6-3 Aza-Aoba, Aramaki, Sendai 980-8578, Japan

[d] Chemistry Department, Faculty of Science, Mansoura University, Mansoura, 35516, Egypt

[e] Yusuf Hamied Department of Chemistry, University of Cambridge, Lensfield Road, Cambridge, CB2 1EW, UK

[f] Department of Pure and Industrial Chemistry University of Nigeria, Nsukka, 410001, Enugu State, Nigeria.

[g] Department of Chemistry and Biological Science, College of Science and Engineering, Aoyama-Gakuin University, Fuchinobe, Chuo-ku, Sagamihara, Kanagawa 252-5258, Japan.

[h] Department of Chemistry, Graduate School of Science Hiroshima University, 1-3-1 Kagamiyama Higashihiroshima 739-8526, Japan.

[i] Research & Utilization Division, Japan Synchrotron Radiation Research Institute (JASRI/SPring-8), 1-1-1 Kouto, Sayo, Hyogo 679-5198, Japan

[j] School of Materials Science and Engineering Nankai University, Tianjin 300350, P.R. China.

ABSTRACT: Theoretical calculations are typically utilized for examining intermetallic interactions. However, to validate theory, experimental confirmation of the existence of these interactions is necessary. We synthesized new heterometallic Ln–Pt complexes, NEt_4{[Pt(PhSAc)$_4$]Ln[(PhSAc)$_4$Pt]}·2DMF (Ln: lanthanoid = Gd (**1**), Tb (**2**), Dy (**3**), PhSAc = benzothioacetate, NEt_4 = tetraethylammonium), in which both diamagnetic Pt(II) ions interact with the central Ln(III) ion. Typically, these interactions are not detected, because the distance between Ln and Pt atoms (~3.6 Å) is much larger than the covalent radius (~3.3 Å) and ionic radius (~3.10 Å). Pt-L_{III} resonant inelastic X-ray scattering (RIXS) analysis was conducted to experimentally confirm the unique influence of the hidden Ln–Pt interaction on the luminescence of the Tb–Pt molecule, where the interaction induced emission properties in the Tb and Pt ions, with high quantum yield (59%). Quantum theory of atoms in molecules (QTAIM) analysis was also used to confirm the experimental results. RIXS analysis allowed the identification of several distinctive characteristics of the coordination environment, including the existence of heterometallic interactions, that affected the observed luminescence.

INTRODUCTION

Heterometallic complexes have been studied in many research fields such as luminescence,[1-3] catalysis,[4-6] and magnetism.[7-14] Luminescence has received particular interest because of its utilization in luminescence devices, bioimaging systems, and photosensitizers. Hasegawa et al. reported the thermo-control emission of a heterometallic Tb(III)–Eu(III) polymer, wherein the energy transfer from the Tb to Eu ion is governed by the thermosensitivity dependence on linker ligands. The luminescence properties of heterometallic complexes have been shown to be modulated by intense heterometallic interactions (e.g., Au–M (M = Ir, Pt, Pd, Ni, and others) complexes).[1] Recently, Roesky et al. conducted theoretical calculations to demonstrate that in a La–Au complex, the shortening of the La–Au distance in an excited state results in the La–Au interaction, which induces photoluminescence.[2] Thus, heterometallic interactions also exert an important influence on the physical properties of heterometallic complexes. Considerable efforts have thus been devoted to the formation of various intermetallic interactions.[1-18] Although high-resolution X-ray diffraction analysis can provide insight into the electron density of bonds,[19] theoretical calculations are widely conducted for examining intermetallic interactions.[1-18]

In this study, we synthesized heterometallic Ln–Pt complexes: NEt_4{[Pt(PhSAc)$_4$]Ln[(PhSAc)$_4$Pt]}·2DMF (Ln: lanthanoid = Gd(**1**),[10] Tb(**2**), Dy(**3**); PhSAc = benzothioacetate, NEt_4 = tetraethylammonium), in which diamagnetic Pt(II) ions interact with the central Ln(III) ions. These interactions are typically overlooked because the Ln–Pt distances are much greater than the covalent radius. The synchrotron Pt-L_{III} resonant inelastic X-ray scattering (RIXS) technique was conducted to observe the electron density of occupied 5d states and heterometallic Ln–Pt bonds to demonstrate the effect of hidden Ln–Pt interactions on the luminescence properties of the complexes. Furthermore, atoms in molecules (AIM) analysis

revealed the existence of weak Ln–Pt interactions. The unprecedented RIXS data for heterometallic complexes provide new insights into the design of heterometallic complexes and all inorganic materials with hidden interactions that impart desirable physical properties (or control the band structure).

Pt-L_{III} RIXS analysis is typically conducted for observing the electronic structures of metal and metal-oxide nanoparticles.[20-23] In Pt-L_{III} RIXS, a 2p state electron is excited to an empty 5d state, then electrons in occupied 5d states fall back to fill the 2p core hole with the emission of photons (X-ray emission). The excited 5d state electron is inelastically de-excited to the lower 5d states (inelastic X-ray scattering: transfer energy). Glatzel et al. observed the CO adsorption of Pt nanoparticles by RIXS analysis, wherein the electronic state or 5d density of states of Pt nanoparticles changed by CO adsorption accompanied by a d-band center was shifted.[20] However, Pt complexes (e.g., cisplatin and its derivatives) exhibited an intensity change that was detected by Pt-L_{III} RIXS analysis, but not a d-band center shift.[24] If RIXS analysis can provide information on structural differences in metal complexes similar to those of bulk-material states of metal and metal-oxide nanoparticles,[21] it will be a crucial method for experimentally confirming heterometallic and metal–ligand interactions in metal complexes. RIXS analysis will be an even more effective method for characterization of general inorganic materials if it allows the identification of more hidden structural differences. Here, we studied the hidden interactions of a new Tb–Pt complex. These interactions are predicted by theoretical calculations. We also demonstrated the advantage of RIXS analysis. Furthermore, the influence of these revealed interactions on the luminescence properties of the Tb–Pt complex was elucidated.

EXPERIMENTAL METHODS

HERFD-XANES and RIXS analyses of powder-sample pellets were carried out in the BL36XU beamline located at SPring-8. Luminescence properties of polycrystalline-solid samples were measured using a Horiba Jobin Yvon GmbH. (Bensheim, Germany) Fluorolog 3–22 spectrofluorometer, Hamamatsu Photonics K. K. (Hamamatsu, Japan) C9920-02 absolute PL quantum yield spectrometer, and Hamamatsu Photonics K. K. (Hamamatsu, Japan) Quantaurus-Tau C11367-12 fluorescence lifetime spectrometer with a pulsed-excitation light source. Theoretical calculations were performed using the Gaussian16 and AIMAll software packages. The simulated density of states (DOS) are calculated with 6 Å radius by FDMNES package under Quadrupole, Relativiste, Spinorbite, Density_all options. Detailed procedures are provided in the Supporting Information (SI).

RESULTS AND DISCUSSION

Complexes **1**, **2**, and **3** are isostructural; therefore, only **2** is shown in Figure 1 (crystal data are summarized in Table S1, CCDC No. 2054548, 2121157, 2121159). Complex **2** had a crystal structure in the *Cc* space group that involves two Pt ions, one Tb ion, eight $PhSAc^-$ ligands, one NEt_4 counteraction, and two DMF crystalline solvent molecules per asymmetric unit. The Tb ion forms a paddle-wheel-like structure with each Pt ion ($\{[Pt(PhSAc)_4]Tb[(PhSAc)_4Pt]\}^-$). Eight O atoms and two Pt ions were coordinated to the Tb ion to form a D_{4d} bicapped square antiprism geometry, as determined using SHAPE 2.1 software.[25] Each Pt ion was coordinated to four sulfur atoms and one Tb ion in a square pyramidal geometry (Figure S1). The intramolecular Tb–Pt distances were 3.608(7) and 3.627(7) Å, respectively. These values are about 10% shorter than the

sum of the atomic radii (4.02 Å), but about 9-17% longer than the covalent (3.30 Å)[26] and ionic (3.10 Å) radii (the reported Tb–Pt bond length is 3.222 Å)[3]. The interaction between Tb and Pt ions is difficult due to the Tb–Pt distance. However, the results of RIXS analysis and AIM calculations show clear evidence of this heterometallic interaction.

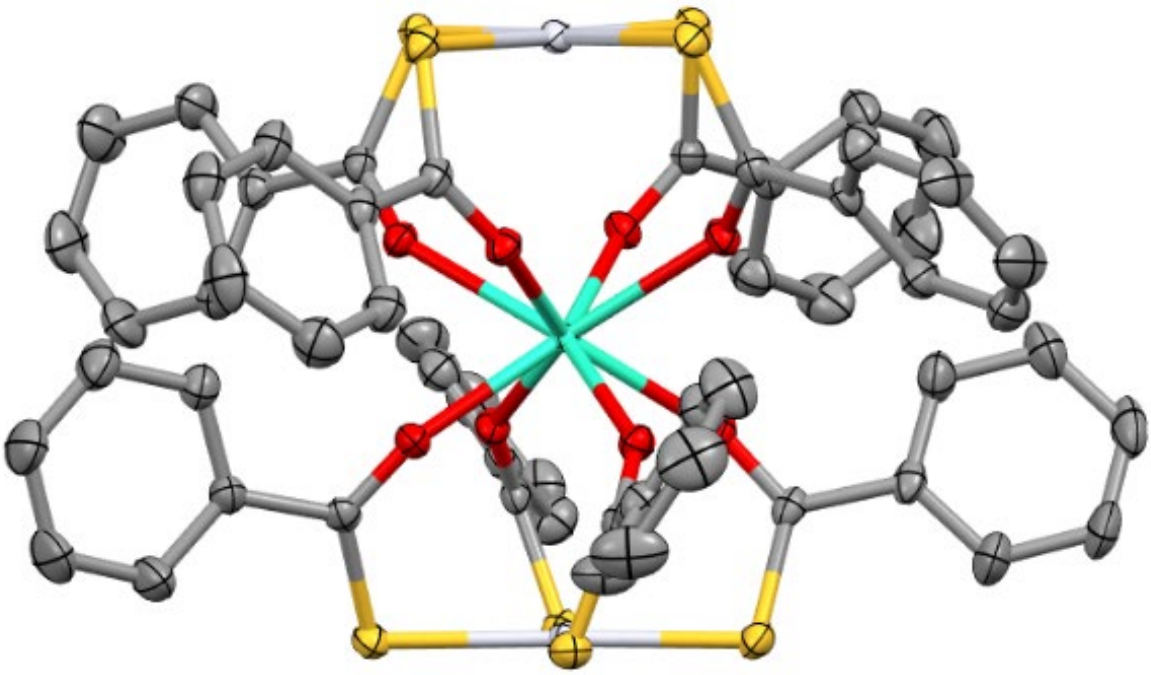

Figure 1. Crystal structure of **2**. White: Pt; green: Tb; grey: C; yellow: S; red: O. Hydrogen atoms have been omitted for clarity.

The high-energy-resolution fluorescence detected X-ray absorption near edge structure (HERFD-XANES) spectra of **1**, **2**, **3**, and $2NBt_4[Pt(dmit)_2]$ at the Pt-L_{III}-edge are shown in Figure S2 (dmit = 3-dithiole-2-dithione). A white line peak assigned to $2p \rightarrow dx^2\text{-}y^2$ absorption shifted slightly from 11568.6 eV for $2NBt_4[Pt(dmit)_2]$) to 11568.7 eV for **1**, 11568.7 eV for **2**, and 11568.8 eV for **3**. The differences in the HERFD-XANES peak positions and shapes among **1**, **2**, **3**, and $2NBt_4[Pt(dmit)_2]$ represent the unoccupied states. However, theoretical calculations[27-28] are required to confirm the coordination geometry in this case.

Two-dimensional (2D) RIXS mapping, which has a higher sensitivity to bonding interactions than XANES, allowed us to observe the Pt–Ln interactions in **1**, **2**, and **3**, but not in $2NBt_4[Pt(dmit)_2]$ (Figures 2b, 2c, and S3). The electronic structure for $2NBt_4[Pt(dmit)_2]$ revealed by 2D RIXS mapping was different in appearance than those of **1–3**. **1–3** each had a clear shoulder peak along the direction of energy transfer (y-axis) (Figures 2 and S3). This difference arises from the DOS induced by the coordination structure around the Pt ions; $2NBt_4[Pt(dmit)_2]$ has a square planar structure and no π stacking (see CCDC 1160680 and CCDC 1204028). Complexes **1–3** have a square pyramidal structure, and their band structures are shown in Figure S1. However, $2NBt_4[Pt(dmit)_2]$ and **1–3** all revealed an inelastic X-ray fluorescence region trailing diagonally from the densest state (~11568 eV and ~4 eV for incident energy and energy transfer, respectively). The aspect of the fluorescence regions indicates the delocalization of electrons.[21] We extracted the difference between the 2D RIXS maps scaled with the maximum z value relative to those of the Gd system, RIXS mapTb-RIXS map_{Gd}, and RIXS mapDy-RIXS map_{Gd}, and compared them in Figure S3 (Δ RIXS at the d-band center = 0; it is noted that there are several ways to scale.). For ΔRIXS $map_{Tb\text{-}Gd}$ (Figure S3c), a greater difference was observed in the higher incident energy region than in the band center. In contrast, the difference between ΔRIXS $map_{Dy\text{-}Gd}$ (Figure S3d)

and ΔRIXS map$_{\text{Tb-Gd}}$ was observed in the area surrounding the band center. The details of these differences are currently under investigation.

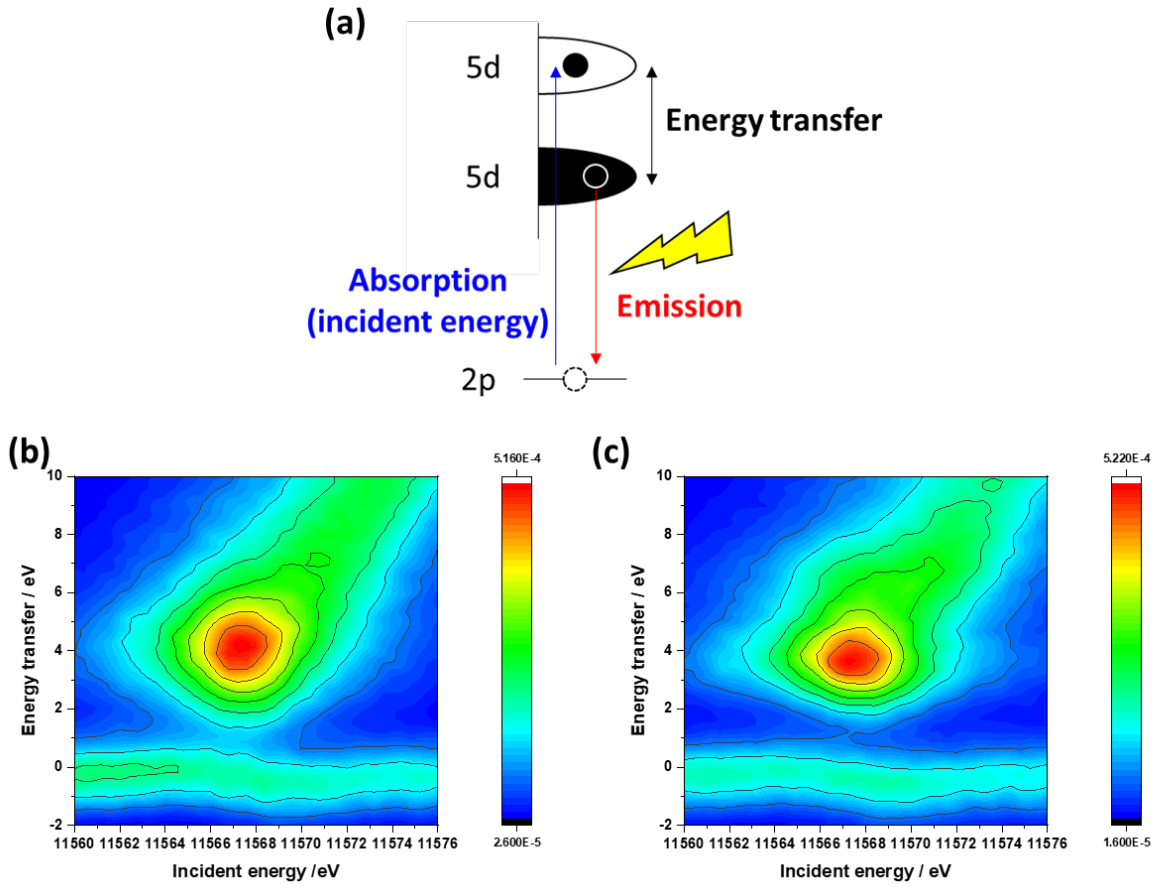

Figure 2. (a) Schematic illustration of RIXS. 2D RIXS maps of (b) 2NBt$_4$[Pt(dmit)$_2$] and (c) **2**.

The energy transfer vs. intensity plots at 11567.3 eV (x axis) of $2NBt_4[Pt(dmit)_2]$ and **2** obtained from the 2D RIXS map are shown in Figure 3. The deconvolution results are summarized in Table 1. As the difference in the RIXS sum spectra between **1**, **2**, and **3** is small, the difference between $2NBt_4[Pt(dmit)_2]$ and **2** is explained here as a typical example. The spectra were deconvoluted into elastic (energy transfer = ~0 eV) and inelastic scattering peaks (Figure S4). The inelastic scattering peaks correspond to the Pt d (at 4.2 eV) and S DOS bands (S sp^2 interacts with Pt 5d at 8.2 eV) for $2NBt_4[Pt(dmit)_2]$, and Pt d DOS (at 3.6 eV) and S DOS bands (S sp^2 interacts with Pt 5d, at 8.3 eV) for **1–3** (Figure S4). These results are consistent with the reported results for Pt-L_{III} RIXS (3 eV and 8 eV, respectively),[21] as well as those of DOS calculations (see Figure S5 and discussion in the SI). In contrast, **1–3** have additional inelastic scattering peaks corresponding to Ln DOS bands (Ln d interacts with Pt 5d at 6.0 eV), which is confirmed by DOS calculations (see Figure S5 and discussion in the SI). These results demonstrate that RIXS analysis allowed the detection of the existence of hidden interactions.

Table 1. Deconvolution results of intensity sum spectra for RIXS map against incident energy for $2NBt_4$ $[Pt(dmit)_2]$, **1**, **2**, and **3**.

	Position (1^{st} peak)	Position (2^{nd} peak)	Position (3^{rd} peak)
$[Pt(dmit)_2]$	4.2 eV	dxy: 8.3 eV	-
1	3.5 eV	5.9 eV	8.5 eV
2	3.6 eV	6.0 eV	8.4 eV
3	3.5 eV	5.9 eV	8.5 eV

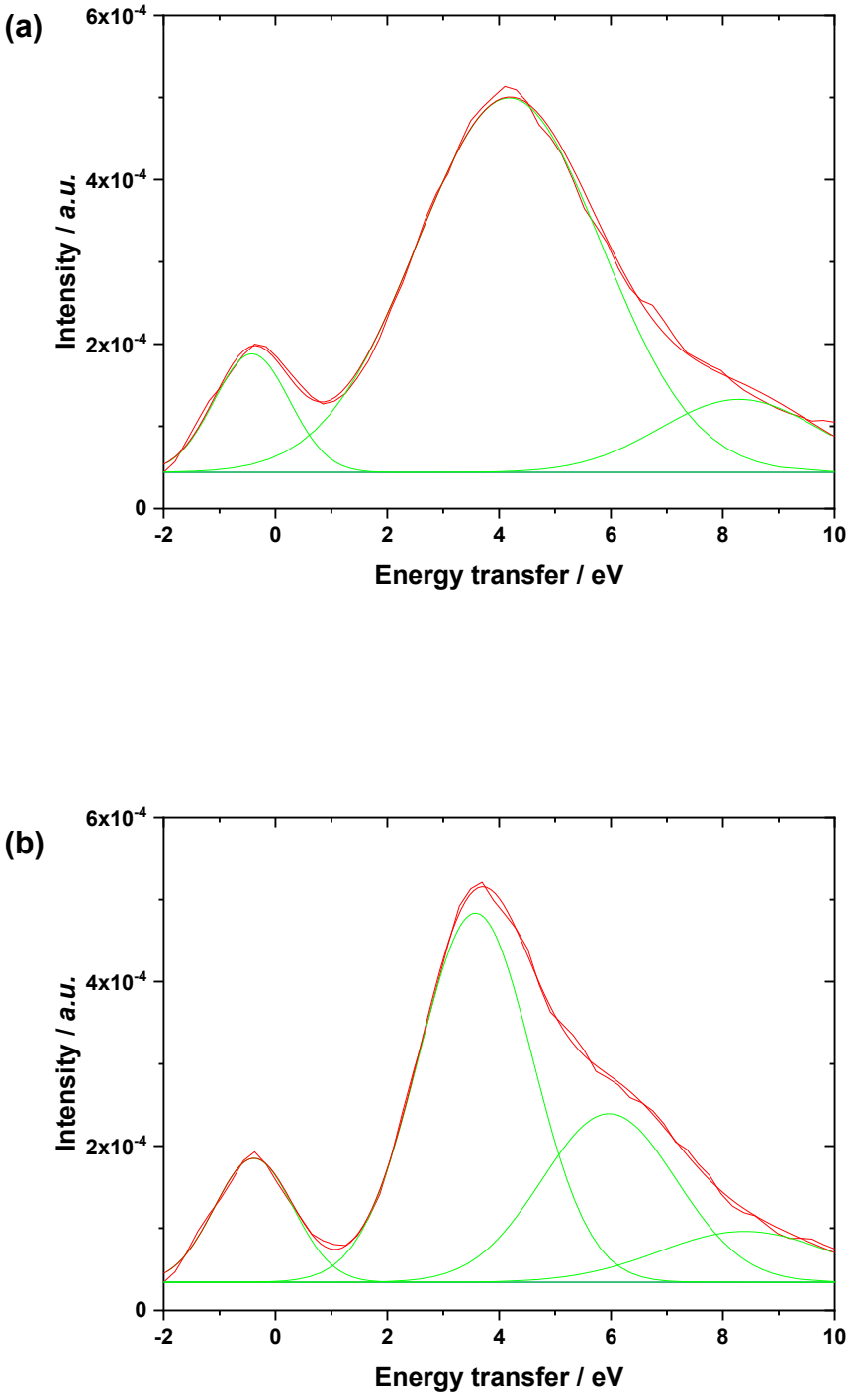

Figure 3. DOS spectrum obtained from the RIXS map of (a) $2NBt_4[Pt(dmit)_2]$ and (b) **2**, and deconvolution peaks**.**

The quantum theory of atoms in molecules (QTAIM) analysis was performed to examine the electron density (ρ) of **1**, **2**, and **3**. In QTAIM, there are typically three critical points where the differential of interatomic ρ is 0, the so-called bond critical points (BCPs). "Bond analysis using QTAIM requires the $\nabla^2\rho$ and E_{total} to have the following relationships: $\nabla^2\rho < 0$ and $E_{total} < 0$ signifies a covalent bond; $\nabla^2\rho > 0$ and $E_{total} < 0$ are values for dative bonds; $\nabla^2\rho > 0$ and $E_{total} = \sim 0$ signals the existent of metallic bond, while $\nabla^2\rho > 0$ and $E_{total} > 0$ indicate a possible ionic bond or van der Waals force of attraction."[29] The word "bond" here has an expanded meaning. Suzuki et al. reported a C–C "bond" whose distance is greater than the van der Waals radii. These "bonds" exhibit an electron density map, and electron density between the C atoms is high. Moreover, this electron density corresponds to that of BCPs.[30] The contour plots on the Pt–Ln–Pt plane and the calculated values of ρ (electron density) and E_{total} (total energy density) are shown in Figure S6, and Table 2, S2 (for **3**, there are no BCPs among Dy and Pt ions, but there are cage critical points (CCPs) between Dy and Pt ions). In Table 2, we use the value of the CCPs instead. According to $\nabla^2\rho$ and E_{total} values, the Ln–Pt bond is between metallic and ionic, whereas Pt–S bonds are dative. In addition, the Ln–Pt bond may be enhanced by bridged ligands because of the presence of ring critical points (Ln–Pt–Ligand 5 member-ring) and CCPs (Ln–Pt–Ligand 8-14 member-ring) among Ln and Pt ions (Figure S6d). Furthermore, Ln–Pt bonds are much weaker than Pt–S bonds, according to the comparison of ρ values. This result indicates that the AIM calculation underestimates ρ_{Ln-Pt}, or RIXS analysis has sufficient sensitivity to observe weak interactions.

Table 2. Calculated QTAIM properties (BCPs) of **2** and **3**.

2	ρ	$\nabla^2\rho$	E_{total}	**3**	ρ	$\nabla^2\rho$	E_{total}
Tb1 - Pt1	0.00796	0.02741	0.00079	Dy1 - Pt1 (CCPs)	0.00762	0.02617	0.00076
Pt1 - S	0.10696	0.14910	-0.04382	Pt1 - S	0.10934	0.15137	-0.04570
	0.10890	0.15075	-0.04534		0.10702	0.14885	-0.04387
	0.10756	0.14971	-0.04428		0.10846	0.14983	-0.04500
	0.10814	0.14899	-0.04474		0.10815	0.15020	-0.04476
Pt2 - S	0.10887	0.15122	-0.04532	Pt2 - S	0.10759	0.15080	-0.04432
	0.10531	0.14678	-0.04254		0.10584	0.14725	-0.04295
	0.10845	0.14991	-0.04498		0.10788	0.14914	-0.04453
	0.10733	0.11498	-0.04412		0.10931	0.15130	-0.04567

As described above, RIXS analysis allowed the clarification of differences in the coordination environment, as well as the existence of heterometallic interactions even for Dy–Pt bonds without BCPs on **3**. These results indicate that RIXS analysis is an essential method for experimentally confirming interactions within metal complexes and inorganic materials.

The diffused reflectance UV/vis absorption spectra of **1**, **2**, and **3** showed peaks at 300 nm and 400 nm and weak peaks at approximately 500 nm (Figure S7). To determine the luminescence properties of **1**–**3**, the emission spectra were measured at 420 nm excitation (The details of the luminescence properties of **3** are shown in the SI). At room temperature (RT, ~300 K), a broad luminescence peak of **1** was observed at 550 nm (Figure S8a). In addition, at 77 K, a similar broad luminescence peak of **1** was observed at 530 nm (Figure 4a). These peaks arise from the phosphorescence of Pt ions (excitation ($S_0 \rightarrow S_1$) → intersystem crossing (ISC; $S_1 \rightarrow T_1$(Pt)) → phosphorescence ($T_1 \rightarrow S_0$)) (Figure S8). The results of the emission lifetime measurement at 77 K (Figure S8b) suggest that there are four emission processes with lifetimes of 0.6, 17.4, 53.8, and 79.7 μs. The observed blue shift at the lower temperature is due to the intensity increment in the higher-wavelength process. These characteristics are similar to the case of the emissions of Pt···Pt dimers that were induced by the similar intense of Ln–Pt interaction, where Ln–Pt distances (~3.6 Å) are much longer than the reported Pt–Pt distance in dimers (*cf.* 3.477(2) Å).[31] This result is consistent with the RIXS measurements. The quantum yields of the region between 450 and 700 nm of **1** at RT and 77 K were estimated to be 0.8 and 18.3%, respectively.

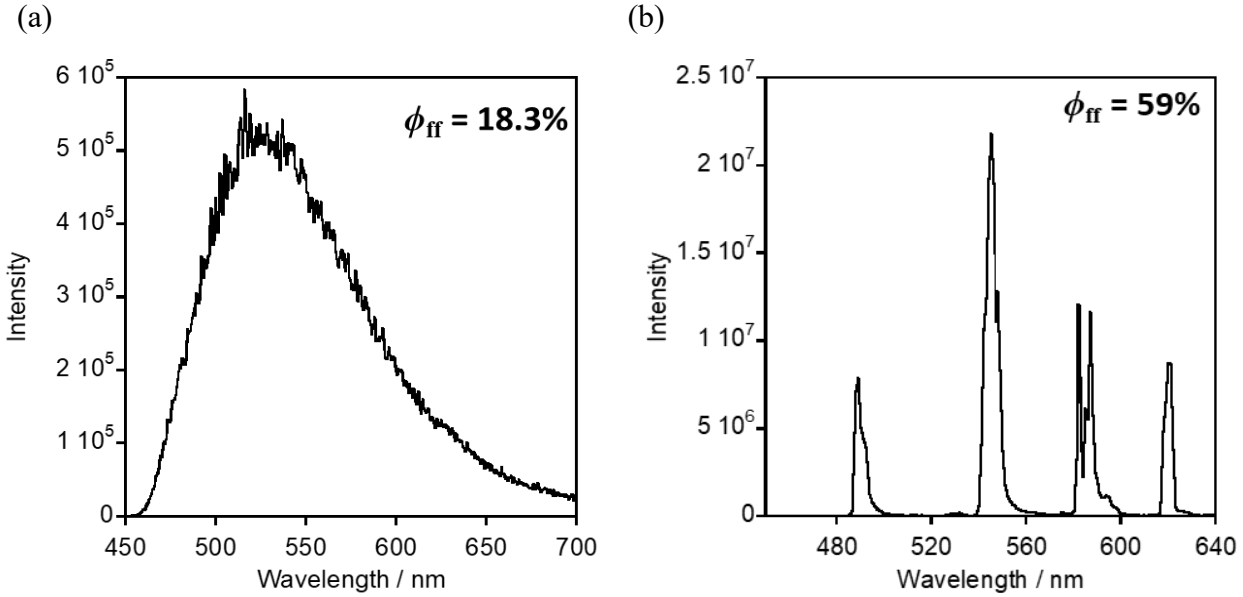

Figure 4. Emission spectra of (a) **1** and (b) **2** at 77 K (λ_{ex} = 420 nm).

For **2,** the observed broad luminescence peak and sharp luminescence peaks (489, 546, 586, and 620 nm) at RT upon excitation at 420 nm originated from the Pt and Tb ions, respectively (Figure S10). Only sharp luminescence peaks (489, 544, 582, and 620 nm) were observed at 77 K (Figure 4b). In addition to the process of **1** from S_0 to T_1 (Pt), energy transfer from T_1 (Pt) to the acceptor level of Tb occurs (Figure S9). Then, emission processes of $^5D_4$ (Tb) to ^7F_n (n = 0, 1, 2, 3, 4, 5, 6) occur. The total CF splitting was calculated as 490 cm^{-1} from the splitting of the $^5D_4$ to $^7F_6$ emission process. There are peaks at 489, 492, 497, and 501 nm, which correspond to the ground $^7F_6$ multiplet (Figure S11). At RT, back-energy transfer from $^5D_4$ (Tb) to T_1 (Pt) occurred (Figure S9). This means that the emissions of the Pt and Tb ions compete. However, at 77 K, back-energy transfer was suppressed, and only the Tb ion emission was observed. The emission lifetime of **2** at 77 K (Figure S12) suggests the possibility of three emissive components (0.017, 1.1, and 3.0 ms). The quantum yields of the region between 450 and 700 nm of **2** at RT and 77 K were estimated to be 0.7% and 59%, respectively. Thus, it was indicated that Pt ions, which interact with the central Tb ion, were an influence on the Tb ion emissions.

The quantum yield of **2** was more than double that of **1** because the energy transfer from the Pt ion to the Tb ion prevents branching into a non-radiative process in the Pt ion. In addition, the yield of **2** is higher than that of the reported heterometallic Tb–Pt complex, because of the higher Tb:Pt ratio for **2** compared to 2:3 for the previously reported complex.[3]

CONCLUSIONS

In summary, RIXS analysis confirmed the hidden interaction between Ln and Pt ions. The differences in the coordination environments of new Pt complexes such as $2NBt_4[Pt(dmit)_2]$ and $NEt_4\{[Pt(PhSAc)_4]Ln[(PhSAc)_4Pt]\}\cdot 2DMF$ were successfully elucidated. Furthermore, the Pt

ions interacted with both sides of the central Tb ion to work as an effective antenna for Tb emissions. These results indicate that RIXS analysis is a versatile experimental tool for providing significant insight into the field of inorganic materials and confirming the existence of hidden interactions that induce desired physical properties (or control the band structure).[32] Additional ΔRIXS-map studies are currently ongoing. In the future, systematic RIXS-related research on topics such as Ln *L*-edge should reveal and define more hidden interactions.

ASSOCIATED CONTENT

Supporting Information

The following files are available free of charge:

General information, synthesis, and experimental section (PDF)

AUTHOR INFORMATION

Corresponding Author

* Takefumi Yoshida - Innovation Research Center for Fuel Cells, The University of Electro-Communications, Chofu, Tokyo 182-8585, Japan, Physical and Chemical Research Infrastructure Group, RIKEN SPring-8 Center, 1-1-1 Kouto, Sayo-cho, Sayo-gun, Hyogo, 679-5148 Japan.

* Masahiro Yamashita - School of Materials Science and Engineering Nankai University, Tianjin 300350, P.R. China, Department of Chemistry, Graduate School of Science Tohoku University, 6-3 Aza-Aoba, Aramaki, Sendai 980-8578, Japan.

Notes

The manuscript was written through the contributions of all authors.

The authors declare no competing financial interests.

ACKNOWLEDGMENTS

This research was supported by JSPS KAKENHI Grant Numbers JP19H05631 (MY), JP20K15293 (TY), 20K15041 (HO), and 17H06374 (MH). Prof. M. Yamashita acknowledges the support of 111 projects (B18030) from China. HERFD-XANES and RIXS measurements were performed at the BL36XU beamline at SPring-8. Part of the work was supported by the New Energy and Industrial Technology Development Organization (NEDO). We would like to thank Editage (www.editage.com) for English language editing.

REFERENCES

[1] Fernández, E. J.; Laguna, A.; López-de-Luzuriaga, J. M., Gold–heterometal complexes. Evolution of a new class of luminescent materials. *Dalton Trans.* **2007,** (20), 1969–1981.

[2] Dahlen, M.; Reinfandt, N.; Jin, C.; Gamer, M. T.; Fink, K.; Roesky, P. W., Hetero-bimetallic Lanthanide-Coinage Metal Compounds Featuring Possible Metal-Metal Interactions in the Excited State. *Chem. Eur. J.* **2021**, *27*, 15128–15136.

[3] Yoshida, T.; Izougu, D. C.; Iwasawa, D.; Ogata, S.; Hasegawa, M.; Breedlove, B. K.; Cosquer, G.; Wernsdorfer, W.; Yamashita, M., Multiple Magnetic Relaxation Pathways and Dual-Emission Modulated by a Heterometallic Tb-Pt Bonding Environment. *Chem. Eur. J.* **2017,** *23*, 10527–10531.

[4] Xu, X.; Luo, G.; Mehmood, A.; Zhao, Y.; Zhou, G.; Hou, Z.; Luo, Y., Theoretical Mechanistic Studies on Redox-Switchable Polymerization of Trimethylene Carbonate

Catalyzed by an Indium Complex Bearing a Ferrocene-Based Ligand. *Organometallics* **2018**, *37*, 4599–4607.

[5] Zhao, X.; Wang, F.; Kong, X.-P.; Fang, R.; Li, Y., Dual-Metal Hetero-Single-Atoms with Different Coordination for Efficient Synergistic Catalysis. *J. Am. Chem. Soc.* **2021,** *143*, 16068–16077.

[6] Patra, S.; Maity, N., Recent advances in (hetero)dimetallic systems towards tandem catalysis. *Coordination Chemistry Reviews* **2021,** *434*, 213803.

[7] Macaluso, E.; Rubín, M.; Aguilà, D.; Chiesa, A.; Barrios, L. A.; Martínez, J. I.; Alonso, P. J.; Roubeau, O.; Luis, F.; Aromí, G.; Carretta, S., A heterometallic [LnLn′ Ln] lanthanide complex as a qubit with embedded quantum error correction. *Chem. Sci.* **2020,** *11*, 10337–10343.

[8] Darago, L. E.; Boshart, M. D.; Nguyen, B. D.; Perlt, E.; Ziller, J. W.; Lukens, W. W.; Furche, F.; Evans, W. J.; Long, J. R., Strong Ferromagnetic Exchange Coupling and Single-Molecule Magnetism in MoS43-Bridged Dilanthanide Complexes. *J. Am. Chem. Soc.* **2021,** *143*, 8465–8475.

[9] Beach, S. A.; Guillet, J. L.; Lagueux, S. P.; Perfetti, M.; Livesay, B. N.; Shores, M. P.; Bacon, J. W.; Rheingold, A. L.; Arnold, P. L.; Doerrer, L. H., Heterotrimetallic {LnOVPt} complexes with antiferromagnetic Ln–V coupling and magnetic memory. *Chem. Commun.* **2020,** *56*, 11062–11065.

[10] Yoshida, T.; Shabana A.; Zhang H.; Chukwuma Izuogu D.; Sato T.; Fuku K.; *et al.* Insight into the Gd–Pt Bond: Slow Magnetic Relaxation of a Heterometallic Gd–Pt Complex. *Bull. Chem. Soc. Jpn.*, **2022**, . 10.1246/bcsj.20210429.

[11] Feng, G.; McCabe, K. N.; Wang, S.; Maron, L.; Zhu, C., Construction of heterometallic clusters with multiple uranium–metal bonds by using dianionic nitrogen–phosphorus ligands. *Chem. Sci.* **2020,** *11*, 7585–7592.

[12] Burns, C. P.; Yang, X.; Wofford, J. D.; Bhuvanesh, N. S.; Hall, M. B.; Nippe, M., Structure and Magnetization Dynamics of Dy−Fe and Dy−Ru Bonded Complexes. *Angew. Chem. Int. Ed.* **2018,** *57*, 8144–8148.

[13] Izuogu, D. C.; Yoshida, T.; Cosquer, G.; Asegbeloyin, J. N.; Zhang, H.; Thom, A. J. W.; Yamashita, M., Periodicity of Single ‐ Molecule Magnet Behaviour of Heterotetranuclear Lanthanide Complexes Across the Lanthanide Series: A Compendium. *Chem. Eur. J.* **2020,** *26*, 6036–6049.

[14] Yoshida, T.; Izuogu, D. C.; Zhang, H.; Cosquer, G.; Abe, H.; Wernsdorfer, W.; Breedlove, B. K.; Yamashita, M., Ln-Pt Electron Polarization Effects on the Magnetic Relaxation of Heterometallic Ho- and Er-Pt Complexes. *Dalton Trans.* **2018,** *48*, 7144–7149.

[15] Shi, K.; Douair, I.; Feng, G.; Wang, P.; Zhao, Y.; Maron, L.; Zhu, C., Heterometallic Clusters with Multiple Rare Earth Metal–Transition Metal Bonding. *J. Am. Chem. Soc.* **2021**, *143*, 5998–6005.

[16] Wächtler, E.; Gericke, R.; Block, T.; Pöttgen, R.; Wagler, J., Trivalent Antimony as L-, X-, and Z-Type Ligand: The Full Set of Possible Coordination Modes in Pt–Sb Bonds. *Inorg. Chem.* **2020**, *59*, 15541–15552.

[17] Cui, P.; Xiong, C.; Du, J.; Huang, Z.; Xie, S.; Wang, H.; Zhou, S.; Fang, H.; Wang, S., Heterobimetallic scandium–group 10 metal complexes with LM→ Sc (LM = Ni, Pd, Pt) dative bonds. *Dalton Trans.* **2020,** *49*, 124–130.

[18] Yang, X.; Burns, C. P.; Nippe, M.; Hall, M. B., Unsupported Lanthanide–Transition Metal Bonds: Ionic vs Polar Covalent? *Inorg. Chem.* **2021,** *60*, 9394–9401.

[19] Krause, L.; Tolborg, K.; Gronbech, T. B. E.; Sugimoto, K.; Iversen, B. B.; Overgaard, J., Accurate high-resolution single-crystal diffraction data from a Pilatus3 X CdTe detector. *J. Appl. Cryst.* **2020,** *53*, 635–649.

[20] Glatzel, P.; Singh, J.; Kvashnina, K. O.; van Bokhoven, J. A., In Situ Characterization of the 5d Density of States of Pt Nanoparticles upon Adsorption of CO. *J. Am. Chem. Soc.* **2010,** *132*, 2555–2557.

[21] Jarrige, I.; Ishii, K.; Matsumura, D.; Nishihata, Y.; Yoshida, M.; Kishi, H.; Taniguchi, M.; Uenishi, M.; Tanaka, H.; Kasai, H.; Mizuki, J. i., Toward Optimizing the Performance of Self-Regenerating Pt-Based Perovskite Catalysts. *ACS Catalysis* **2015,** *5*, 1112–1118.

[22] Singh, J.; Nelson, R. C.; Vicente, B. C.; Scott, S. L.; van Bokhoven, J. A., Electronic structure of alumina-supported monometallic Pt and bimetallic PtSn catalysts

under hydrogen and carbon monoxide environment. *Phys. Chem. Chem. Phys.* **2010,** *12*, 5668–5677.

[23] Uruga, T.; Tada, M.; Sekizawa, O.; Takagi, Y.; Yokoyama, T.; Iwasawa, Y., SPring-8 BL36XU: Synchrotron Radiation X-Ray-Based Multi-Analytical Beamline for Polymer Electrolyte Fuel Cells under Operating Conditions. *The Chemical Record* **2019**, *19*, 1444–1456.

[24] Lipiec, E.; Czapla, J.; Szlachetko, J.; Kayser, Y.; Kwiatek, W.; Wood, B.; Deacon, G. B.; Sá, J., Novel in situ methodology to observe the interactions of chemotherapeutical Pt drugs with DNA under physiological conditions. *Dalton Trans.* **2014**, *43*, 13839–13844.

[25] SHAPE2.1 Released 2013-3: Llunell, M.; Casanova, D.; Cirera, J.; Alemany, P.; Alvarez, S., Universitat de Barcelona, Barcelona, 2013.

[26] Cordero, B.; Gomez, V.; Platero-Prats, A. E.; Reves, M.; Echeverria, J.; Cremades, E.; Barragan, F.; Alvarez, S., Covalent radii revisited. *Dalton Trans.* **2008,** (21), 2832–2838.

[27] Rehr, J. J.; Kas, J. J.; Vila, F. D.; Prange, M. P.; Jorissen, K., Parameter-free calculations of X-ray spectra with FEFF9. *Phys. Chem. Chem. Phys.* **2010**, *12*, 5503–5513.

[28] Bunau, O.; Joly, Y., Self-consistent aspects of x-ray absorption calculations. *J. Phys.: Condens. Matter.* **2009**, *21*, 345501.

[29] Vlaisavljevich, B.; Miró, P.; Cramer, C. J.; Gagliardi, L.; Infante, I.; Liddle, S. T., On the Nature of Actinide–and Lanthanide–Metal Bonds in Heterobimetallic Compounds. *Chem. Eur. J.* **2011**, *17*, 8424–8433.

[30] Ishigaki, Y.; Shimajiri, T.; Takeda, T.; Katoono, R.; Suzuki, T., Longest C–C Single Bond among Neutral Hydrocarbons with a Bond Length beyond 1.8 Å. *Chem* **2018,** *4*, 795–806.

[31] Saito, D.; Ogawa, T.; Yoshida, M.; Takayama, J.; Hiura, S.; Murayama, A.; Kobayashi, A.; Kato, M., Intense Red-Blue Luminescence Based on Superfine Control of Metal–Metal Interactions for Self-Assembled Platinum(II) Complexes. *Angew. Chem. Int. Ed.* **2020,** *59*, 18723–18730.

[32] Gould, C. A.; McClain, R. A.; Reta, D.; Kragskow, J. G. C.; Marchiori, D. A.; Lachman, E.; Analytis, J. G.; Britt, R. D.; Chilton, N. F.; Harvey, B. G.; Long, J. R., Ultrahard Magnetism from Mixed-Valence Dilanthanide Complexes with Metal-Metal Bonding. *Science* **2022**, *375*, 198–202.

TOC GRAPHIC